RSC Advances

ROYAL SOCIETY OF CHEMISTRY

www.rsc.org/advances

Comprehensive study of the adsorption of an acylhydrazone derivative by serum albumin: An unclassical static quenching

Jin-Qiang Tong[a], Fang-Fang Tian[b], Yi Liu[a,b,*], Feng-Lei Jiang[b,*]

[a] College of Chemical and Environmental Engineering, Yangtze University, Jinzhou 434023, P. R. China

[b] State key laboratory of Virology & Key laboratory of Analytical Chemistry for Biology and Medicine (MOE), College of Chemistry and Molecular Sciences, Wuhan University, Wuhan 430072, P. R. China

*Corresponding author: Prof. Dr. Yi Liu & Prof. Dr. Feng-Lei Jiang

E-mail: yiliuchem@whu.edu.cn (Y. Liu); fljiang@whu.edu.cn (F.L. Jiang).

Tel & Fax: +86 27 68756667.

Abstract

In this study, an acylhydrazone derivative, named N'-(2-chlorobenzylidene)-2-hydroxybenzo-hydrazide (NCH) had been synthesized by a one-pot synthesis method. Spectroscopy together with molecular modeling and electrochemistry were employed to investigate the binding behavior of NCH to serum albumin (SA), including human serum albumin (HSA) and bovine serum albumin (BSA), under the physiological conditions. An unclassical static quenching had been proven in the fluorescence quenching of SA induced by NCH, due to the large activation energy requirement in the binding process. NCH was absorbed to both HSA and BSA with a 10^4 M^{-1} affinities constant. The primary binding driving force was the typical hydrophobic interaction occurring in Sudlow's site I of SA, while hydrogen bonds stabilized the NCH-SA complex and fixed NCH configuration in binding pocket. NCH could slightly destroy the polypeptides backbone and change α-helix into unordered ribbon. It was shown that NCH could efficiently bind with SA.

Keywords: acylhydrazone, Serum Albumin, interactions, the static fluorescence quenching, Surflex Dock

1. Introduction

Acylhydrazone is a kind of substituted Schiff base, with the common structure of O=C-N-N=C, related to the condensation of aldehyde or ketone with acylhydrazine.[1-4] Acylhydrazone has been a hot topic for a long time and still attracts the interest of scientists now, due to its excellent biological activities.[2,3] Some acylhydrazones have been used as medicine, antiseptic and pesticide for a long time.[4] Recently, scientists find that some acylhydrazones possess significant activities of anticancer[3,4], anti-bacterial[5], anti-HIV[6], anti-convulsant[7] and anti-tubercular[8]. And due to the desirable ability to form coordination complex with metal ions such as Fe^{3+} and Fe^{2+}, some acylhydrazones have been devoting to treatment of the iron overloaded diseases such as β-thalassemia major.[9,10] Some acylhydrazones have been found to possess anti-proliferative ability and can be used as potential anticancer drugs.[3,11] But some key problems of pharmacology and pharmacokinetics are still unrevealed. Here in this study, we used N'-(2-chlorobenzylidene)-2-hydroxybenzo-hydrazide (NCH) as a model to detect the behaviors of acylhydrazones in human body, and we paid our attention in biological effect to provide valuable information to the concerns regarding the biological effects of acylhydrazone.

The binding behaviors of drug to plasma protein is an important and dominating factor to understand the pharmacodynamic and pharmacokinetics properties of drug, because the binding properties largely determine the drug transportation and distribution.[12] HSA, the most prominent protein in human plasma, shows the capability to bind a wide range of endogenous and exogenous ligands, such as fatty

acids, heme, free metal ions, as well as an extraordinarily broad range of drugs.[10,13-15] Based on the crystallographic analysis, HSA is a 585 amino acid residue monomer, and contains three homologous α-helical domains (I-III), and each of them is composed by two sub-domains A and B.[16] The crystal structure analysis also indicates that the principal regions of ligand binding sites in HSA are located in hydrophobic cavities in sub-domains IIA and IIIA. These binding sites are known as Sudlow site I and Sudlow site II, respectively, and the sole tryptophan residue in HSA is located in Sudlow I (Trp-214).[17,18] The hydrophobic cavities in HSA generally increase the apparent solubility of hydrophobic drug in plasma and modulates the delivery of drug to cells in vivo and in vitro, so they play an important role in drug binding, especially for the lipophilic drug.

BSA is a heart-shaped helical monomer which is made up of three homologous domains called I-III, with each domain including two sub-domains named A and B to form a cylinder. BSA shares ~80% homologous amino acid sequences with HSA, so their structures are similar and they have equivalent binding site for many endogenous and exogenous ligands.[1,12,13] There are two tryptophan residues interesting to us. The first one is Trp156, which is embedded in the first sub-domain IB and is exposed to a hydrophilic environment. The second one is Trp237, which is deeply buried in the hydrophobic loop in sub-domain IIA .[1,14]

As we know, the binding of a drug to SA usually conduces the quench of SA's intrinsic fluorescence. Usually, the quenching process can be divided into classical static quenching and classical dynamic quenching.[1,16,18] The static quenching is

mainly induced by the ground-state complex formation process between the quencher and fluorescent chromophore. However, the dynamic quenching is mainly caused by the collision between the excited protein and drug.[17-19] In both ways, energy can be transferred from excited protein to the drug thus quench the fluorescence emission. These two quenching mechanisms can be distinguished by several methods: the dependence of quenching constant on temperature, the change of absorption spectrum of protein and the lifetime of excited protein.[18,19] As to the temperature dependence, the quenching constant increases with the rising temperature for dynamic quenching, since the diffusion is the control step in this mechanism. Whereas, the opposite dependence will be found in static quenching, because the stability of the complex decreases with the rising temperature.

We reported here this study of interactions between NCH and SA under physiological condition systematically and comprehensively using various molecular docking, spectroscopy and electrochemical methods. This study may provide valuable information to the growing concerns of pharmacy and biophysical properties of acylhydrazone and its analogies, as well as the biological side effects of hydrazone based drug on organism and human body.

2. Experimental Section

2.1 Reagent and Apparatus

The reactants and solvents used in synthesis were obtained from Sinopharm Chemical Reagent Co. Ltd., and all of them were analytical reagent grade and used as

received. NCH was dissolved in ethanol at the concentration of 40mM as stock solution and kept in refrigerator at 4 ^{o}C, and then diluted before use. HSA and BSA were purchased from Sigma Aldrich and dissolved in PBS (pH = 7.4) a day before use and kept in refrigerator at 4 ^{o}C. Water used in all the procedures was obtained from a Millipore water purification system.

Fluorescence spectra were measured using a LS-55 spectrofluorophotometer from Perkin Elmer equipped with a thermostat bath. A UNICO 4802 UV-vis Double Beam Spectrophotometer was used to measure absorption spectra of NCH and the NCH-SA system. The electrochemical experiments were performed on a CHI660C electrochemical workstation from Shanghai Chenhua Instrument Company. For the synthesis and identification, element analysis was performed with an Elementar Aralysensysteme GmbH VarioEL elemental analysis system. Infrared spectra were measured on an Avatar 360 FT-IR spectrophotometer as KBr pellets.

2.2 Preparation

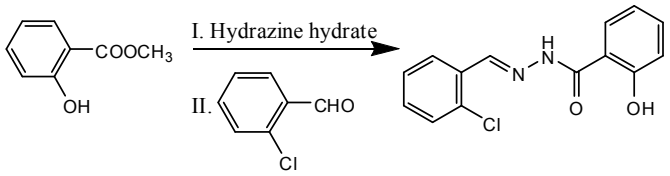

Scheme 1 The synthesis route to NCH

As showed in Scheme 1, hydrazine hydrate (85%, 2.0 mmol) was added to a solution of methyl 2-hydroxybenzoate (2.0 mmol) in ethanol (20 mL). Then approximately 0.05 mL acetic acid was added as catalyst. The reaction mixture was stirred and refluxed. When the reaction was finished monitoring by the TLC, a

solution of 2-chloro-benzaldehyde (2.0 mmol, ethanol, 10 mL) was added dropwise. The mixture was refluxed for 3h, cooled down naturally and then stored in refrigerator at -20 ^{o}C overnight. The precipitation was collected, washed and recrystallized. The final product was a white powder with a total yield of 82%. Elemental analysis: found (cal.): C 61.57(61.21); H 4.15(4.04); N 10.36(10.20); ^{1}H NMR (400 MHz; in DMSO-d_6): δ=12.09 (s, 1H; N*H*), 11.79 (s, 1H, o-O*H*), 8.87 (s, 1H, N=C*H*), 8.06-6.96 (m, 8H, Ar-*H*). IR: 3420 cm^{-1}(s, O-H), 1640(s, C=O), 1550(s, C=N), 1490, 1450, 1380(m, Ar), 1230(m, =C-H), 1150(m, Ar-O), 752, 686(m, 1,2-substituted Ar). UV-Visible (in PBS; $L \cdot mol^{-1} \cdot cm^{-1}$): 216 nm($2.34 \times 10^4$).

2.3 Measurements

The fluorescence spectra were measured using a 1 cm quartz cell at 313, 308, 303 and 298 K. The excitation wavelength was set at 280nm with a 15/12 nm excitation and emission slit. Very dilute solution of SA (2 μM) and NCH (0 - 5 μM) were used, in order to avoid inner filter effect in all fluorescence spectra measurements.[1,9,19] The site competitive experiments were conducted as adding NCH to SA-site marker system.[1,9,19-21] The UV-visible absorption spectra were measured with a 1 cm quartz cell at room temperature.

A three-electrode electrochemical system was employed in the experiments of electrochemistry. The working electrode was a gold disk electrode (diameter = 2 mm), while Ag/AgCl electrode served as reference electrode with a Pt wire counter electrode. The preparation of SA modified working electrode was based on the dry adsorption method developed in former work, while the test conditions were also

similar with preview publications.[9,22,23]

2.5 Molecular docking investigation

The molecular structure of NCH was drawn in Sybyl 8.1 and then charged with Gasteiger-Marsili method. Then the energy and geometry were optimized by Powell method. The detailed parameters were: Initial Optimization: Simplex; Termination: Gradient at 0.01 Kcal/mol; Force Field: Tripos; Other parameters were using the default setting.

The crystal structures of HSA employed in the molecular docking study were downloaded from PDB database, and their PDB ID were 1H9Z and 2BXG, respectively. The crystal structure 1H9Z contained a warfarin and five fatty acid molecules, and they were all extracted before docking study. While 2BXG was a bimolecular crystal and contained an exogenous ligand ibuprofen, and chain b and ligand were removed before docking. And then the whole structure was prepared for docking with Sybyl 8.1 software.

The 3D structure of BSA was modeled using Modeller_9v7, the detailed process was described in our previous work.[1] For short, BSA was modeled using the crystal structure HSA (PDB entry: 1ao6) as a temple molecule. And then, the structure was analyzed and treated with Sybyl 8.1 software. The rms deviation (RMSD) corresponding to equivalent C-α atoms in BSA model and HSA structure is 0.303 Å. The final structure was used for the Surflex Dock program.

Docking study was conducted by a Surflex Dock program in Sybyl 8.1 package. The protomol for HSA was generated by AUTO and LIGAND mode, while warfarin

and ibuprofen were selected as the ligand in LIGAND mode. The protomol for BSA was generated by AUTO and RESIDUE mode, while Trp237 were selected as the core residue in RESIDUE mode. After using different parameters to model the interaction of NCH to SA, we chose the results with the highest score to discuss the most possible binding site and binding conformation.

3. Results and Discussion

3.1 Fluorescence quenching study

Fluorescence spectroscopy is a widely used technology in the research fields involving the fluorescent biomacromolecules.[24,25] Fluorescence quenching is a direct results of the reducing of the quantum yield of fluorescent substances.[21] Fluorescence quenching study can provide various information, such as quenching constant, binding constant, quenching mechanism, binding number, binding driving force, and so on. So we employed fluorescence quenching in studying the interactions between NCH and SA.

Fluorescence titration measurements were carried out to determine whether NCH could interact with SA or not. As illustrated in Fig. 1[A], HSA gives a strong emission band at around 349 nm, while NCH almost gives no emission under this condition. So the emission is direct related to the behavior of HSA. The fluorescence intensity of HSA decreases acutely and regularly with continuous addition of NCH. This indicates the exogenous NCH quenches the intrinsic fluorescence of HSA and this quenching effect is obviously positively related to the concentration of NCH. The similar situation happens in NCH-BSA system, as showed in Fig.1[C]. As the addition

of NCH, the emission band of BSA at around 350 nm drops rapidly and the quenching is positively related to the concentration of NCH. These experiments demonstrate the NCH can effectively interact with SA and quench their intrinsic fluorescence emission.

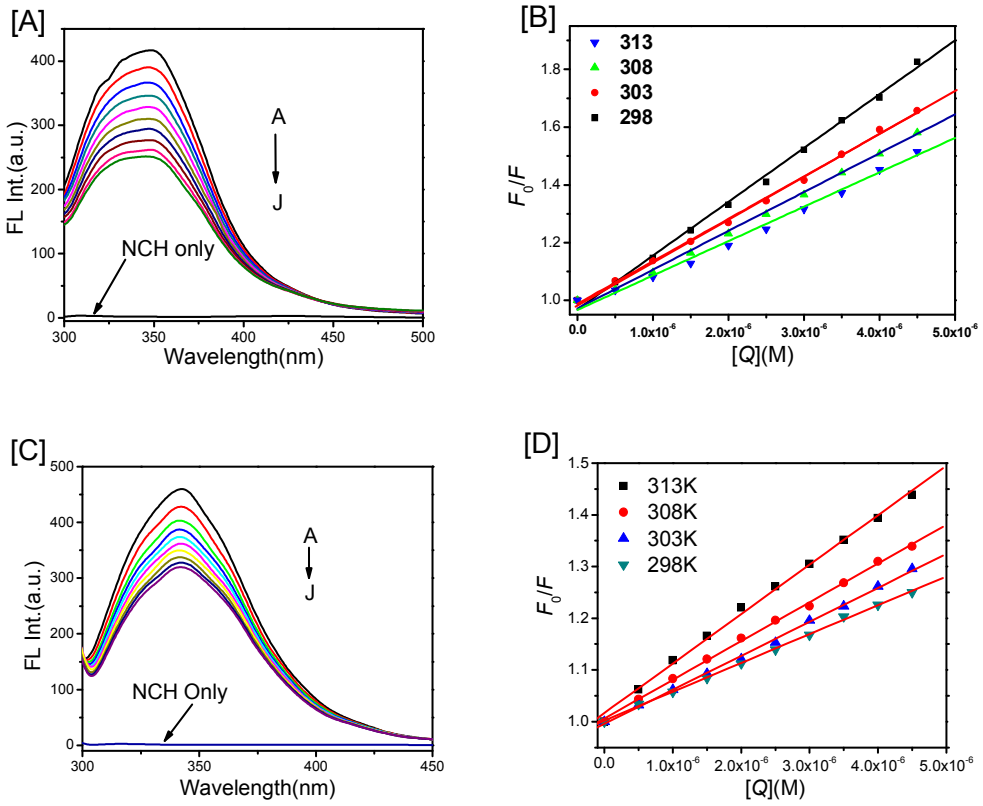

Fig. 1 The fluorescence titration spectra of NCH to SA at 308K, Stern-Volmer plots at each temperature.

[A]&[B]: NCH-HSA; [C]&[D]: NCH-BSA; The concentration from A to J is: 0, 0.5, 1.0, 1.5, 2.0, 2.5, 3.0, 3.5, 4.0, 4.5μM. The curve in the bottom shows the emission spectrum of NCH only in this condition.

In order to reveal fluorescence quenching mechanism, fluorescence quenching had been performed at different temperatures to distinguish the quenching mechanism by

the temperature dependence. As concluded before, the quenching constant will decrease in static quenching with the rising temperature, while the opposite effect can be detected in dynamic quenching.[5,7,26-29] The quenching constant can be calculated by the Stern-Volmer equation (Equation 1) in each temperature:

$$\frac{F_0}{F} = 1 + K_{sv}[Q] = 1 + k_q \tau_0 [Q] \quad (1)$$

F_0 and F are the fluorescence intensities in the absence and prensence of NCH, respectively. [Q] represents the concentration of NCH, while K_{SV} stands for the quenching constant. τ_0 is the constant average fluorescence lifetime of bimolecular and equals to 10^{-8} s ; k_q, which equals to K_{SV}/τ_0, means the apparent bimolecular quenching rate constant. For dynamic quenching, the maximum scattering collisional quenching constant of various quencher is limited to less than 2.0×10^{10} $L\cdot mol^{-1}\cdot s^{-1}$.[1,9,12,26] Fig. 1[B]&[D] illustrates the Stern-Volmer plots at different temperatures, while K_{SV} and k_q are presented in Table 1.

For both HSA-NCH and BSA-NCH, K_{SV} and k_q decrease with the decreasing temperature, suggesting the fluorescent quenching caused by NCH may be a dynamic quenching. However, k_q for this NCH-SA system is much larger than 2.0×10^{10} $L\cdot mol^{-1}\cdot s^{-1}$, the limitation of the dynamic quenching. Herein, we can't reveal the actual quenching mechanism, because of the conflict of fluorescent data with the classic fluorescent quenching theory. So we employed UV-visible absorption spectroscopy and electrochemical experiments to verify the actual quenching process.

Table 1 The parameters calculated from the Stern-Volmer plots

T (K)	HSA-NCH			BSA-NCH		
	$10^{-5}K_{SV}$ ($L \cdot mol^{-1}$)	$10^{-13}k_q$ ($L \cdot mol^{-1} \cdot s^{-1}$)	R*	$10^{-4}K_{SV}$ ($L \cdot mol^{-1}$)	$10^{-12}k_q$ ($L \cdot mol^{-1} \cdot s^{-1}$)	R*
313	1.66	1.66	0.9969	9.56	9.56	0.9982
308	1.47	1.47	0.9975	7.50	7.50	0.9992
303	1.34	1.34	0.9966	6.56	6.56	0.9991
298	1.19	1.19	0.9920	5.58	5.58	0.9994

*R is the correlation coefficient for Stern-Volmer plots.

In the UV-visible experiments, we conducted a subtracting experiment and an addition experiment. As reported and approved, the absorption spectrum of HSA should have no detectable change if the quenching is a dynamic mechanism.[1,5,24,28] Differently, a ground-state SA-drug complex forms in the static quenching, and the absorption spectrum of SA changes as a direct consequence.[30] As we can see from Fig. 2[A], the UV-visible absorption spectra of HSA, NCH and HSA-NCH system are measured. The absorbance curve of HSA (curve D), comparing to curve B (stand for [(NCH +HSA)-NCH] system), changes significantly in the range of 250 – 400 nm, around both 280 nm (about 0.14 in absorbance) and 210 nm (about 2.3 in absorbance). This change is not caused by the increasing volume of the system (only 0.15%), so it is the reasonable result of the ground-state complex formation of NCH and HSA. The similar phenomenon occurs in BSA-NCH, the results are demonstrated in Fig. 2[B].

Also, we conducted an addition UV-visible spectra experiment, only increasing the NCH concentration, presented in Fig. SI 4[A]&[B] in Supplementary Information. According to the figures, the absorbance in the range of 250 – 400 nm increases

dramatically with the increasing concentration of NCH. This is in accordance with the subtracting spectra: NCH binds to HSA and forms a ground-state complex, and in this way the spectrum of HSA has been changed. The more the complex forms, the more the absorption spectra changes. The same results can be got easily according to the addition UV spectra of NCH to BSA. Therefore, according to UV-visible spectroscopy, the fluorescence quenching of SA induced by NCH is primarily caused by NCH-SA complex formation.

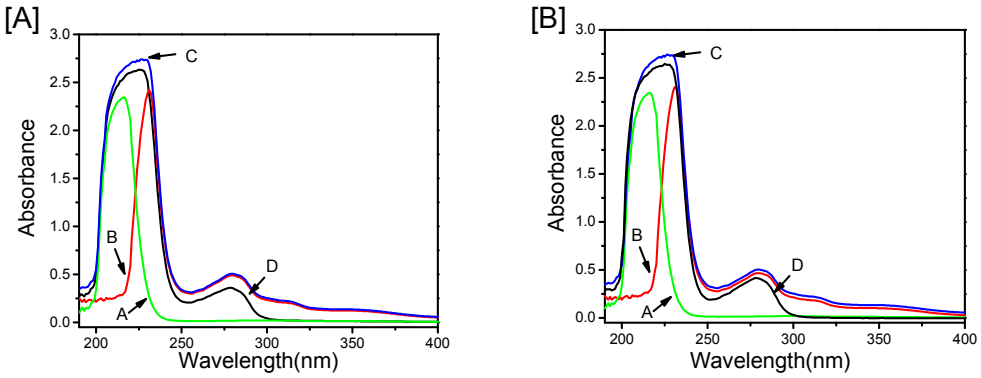

Fig. 2 UV-visible subtracting spectra of HSA-NCH[A] and BSA-NCH[B].

[A]: Curve A, B, C and D stands for NCH only, [(NCH +HSA)- NCH], [NCH +HSA], and HSA only, respectively. *c*(HSA) = *c*(NCH) = 10μM. [B]: Curve A, B, C and D stands for NCH only, [(NCH +BSA)- NCH], [NCH +BSA], and BSA only, respectively. *c*(BSA) = *c*(NCH) = 10μM

The electrochemical analysis is widely utilized in studying the interactions between bioactive ligands and biomacromolecules. Here, we employed electrochemical impedance spectroscopic (EIS) experiments to verify the binding process of NCH into SA and to provide some experimental evidences besides spectroscopy. We used a dry adsorption method to immobilize the SA molecules onto working electrode surface,

which was developed in our group.[9,22,23] When we compared the EIS of blank Au electrode (Fig. 3[A]) with the HSA modified electrode (Fig. 3[B] curve A), we can easily know that the R_{ct} of bare Au electrode is very small (calculated to be 320Ω), while the R_{ct} value of HSA modified Au electrode is large (about 4059Ω). Based on this comparison, we are sure that HSA has been actually immobilized onto the surface of Au electrode therefore blocking the electronic current transportation, causing the R_{ct} increase. When adding NCH to the electrochemical system, as showed in Fig. 3[B]&[C], R_{ct} increases continuously with the increasing NCH. This declares NCH continuously binds to HSA on the surface of Au electrode and increases the resistance. This means the binding of NCH towards SA on Au surface is the primary interaction pattern of the NCH-SA system, instead of collision.

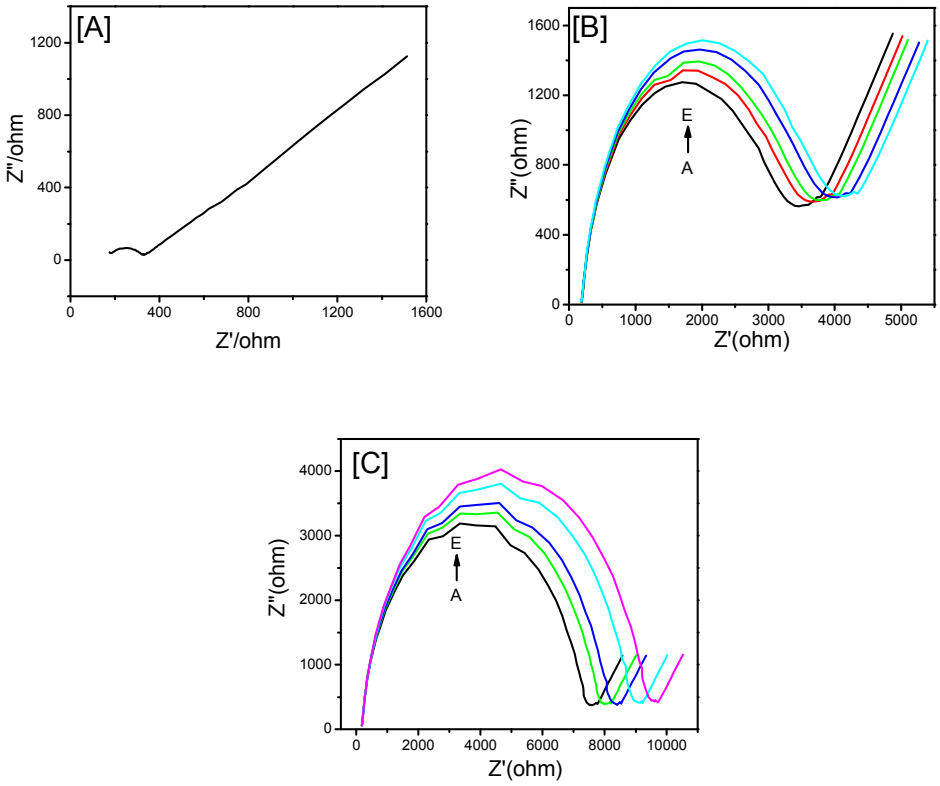

Fig. 3 Electrochemical impedance spectroscopy of bare Au electrode[A], HSA-NCH[B] and BSA-NCH[C] system.

Various concentration of NCH interact with and SA. The concentration of NCH for A-E (μM): 0, 2.0, 4.0, 6.0, 8.0.

We utilized the Langmuir isotherm model(Equation 2)[31] to calculate the constant binding parameters:

$$K_a c = \frac{R_{ct(i)} - R_{ct(0)}}{R_{ct(0)}} \qquad (2)$$

c stands for the concentration of NCH. $R_{ct(i)}/R_{ct(0)}$ is a linear function of c from which the affinity constant K_a can be obtained as the slope[33-35], which is shown in Fig. SI 5. The value of K_a for HSA and BSA equals to 2.42×10^4 L·mol^{-1} and 2.21×10^4 L·mol^{-1}, respectively.

Based the discussion above, the fluorescence titration experiments together with UV-Visible absorption spectra and EIS experiment, we could conclude that the interactions between NCH and SA are primarily arisen from the NCH-SA complex formation process. In another word, the quenching of SA's intrinsic fluorescence by NCH is mainly by a static quenching mechanism, although unclassical in some extent.

As to the unclassical static quenching, we think it can be explained properly by the Arrhenius' activation theory. According to this theory, the rate constant k is a positive function of temperature, so temperature has a great impact on rate constant. When temperature rises, the complex becomes unstable and tends to dissociate in the classical static quenching theory, whereas the rate constant tends to increase with the

increasing temperature according to Arrhenius' activation theory. If the increase caused by the higher temperature is larger than the decrease leading by the unstable tendency, the total outcome will be the quenching constant increases with temperature.

We calculate the activation energy of quenching process according to the Arrhenius equation (Equation 3) to evaluate the impact of temperature on quenching constant:

$$\ln(K_{sv}/\tau_0) = \ln k_q = -\frac{E_a}{RT} + \ln A \qquad (3)$$

E_a is the activation energy of the quenching reaction; A is the Pre-exponential factor. The plots of $\ln k_q$ versus $1/T$ is a straight line, and the value of E_a can be obtained from the value of slope.[1,23] As presented in Fig. 4, for both HSA-NCH and BSA-NCH system, a good linear relationship implies E_a has no significant change in the experimental temperature range. And the value of E_a is about 19.0 and 27.1 kJ·mol^{-1}, for HSA-NCH and BSA-NCH respectively, and they are bigger than many other bio-molecular reactions,[1, 16-19] proving the impact of temperature on the value of K_{SV} is fateful.

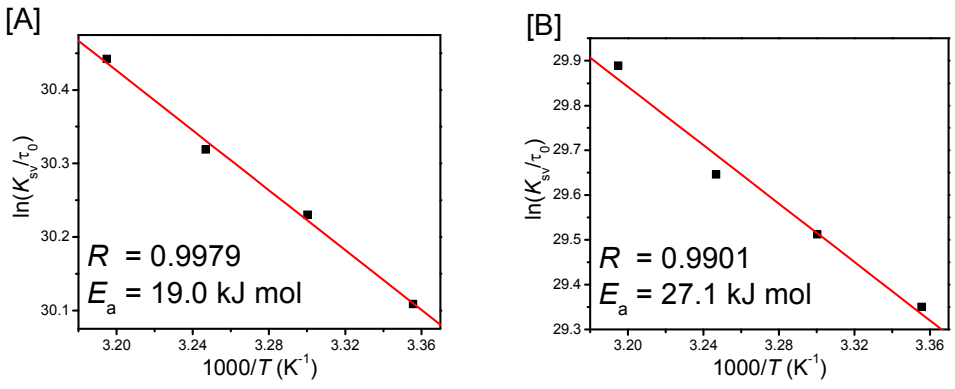

Fig. 4 Arrhenius plots for HSA-NCH[A] and BSA-NCH[B].

3.3 Binding properties of NCH-SA

3.3.1 Binding constant

The quenching is confirmed as a complex formation process, the modified Stern-Volmer equation (Equation 4) is applied to calculate the affinity constant K_a.

$$\frac{F_0}{\Delta F} = \frac{F_0}{F_0 - F} = \frac{1}{f_a K_a}\frac{1}{[Q]} + \frac{1}{f_a} \quad (4)$$

Herein, the f_a is the fraction of accessible fluorescence, and K_a stands for the effective quenching constant. $F_0/\Delta F$ is linear with $1/[Q]$, and slope equals to the value of $(f_a \cdot K_a)^{-1}$. Fig. 5 gives the modified Stern-Volmer plots at various temperatures and the good linear relationship has been showed as well. The corresponding values of K_a and other parameters are exhibited in Table 2. As showed clearly in Table 2, the binding constants for both HSA-NCH and BSA-NCH is about 10^4 L·mol^{-1}, and this is highly coincide with that obtained from EIS calculation.

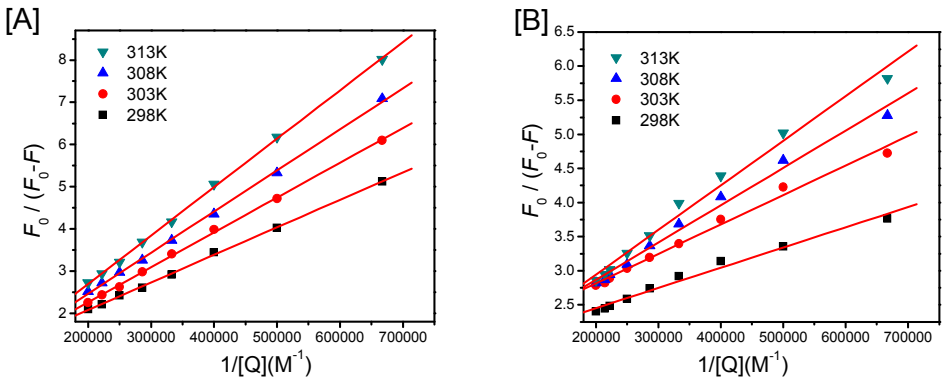

Fig. 5 The modified Stern-Volmer plots for HSA-NCH[A] and BSA-NCH[B] system at different temperatures.

Table 2 The thermodynamic parameters of NCH-SA system

T (K)	$10^{-4}K_a$ (L·mol^{-1})	R^*	n^{**}	ΔH (KJ·mol^{-1})	ΔG (KJ·mol^{-1})	ΔS (J·K^{-1}·mol^{-1})

HSA	313	8.31	0.9996	1.38	45.9	-29.5	161.6
	308	7.38	0.9995	1.37		-28.7	
	303	5.29	0.9994	1.30		-27.3	
	298	3.47	0.9997	1.20		-25.9	
BSA	313	6.28	0.9922	1.61	47.9	-28.7	244.8
	308	4.52	0.9953	1.40		-27.4	
	303	3.23	0.9943	1.33		-26.2	
	298	2.51	0.9931	1.24		-25.1	

*R is the correlation coefficient for Stern-Volmer plots.

**n is the binding number calculated from the double logarithm plots.

3.3.2 Binding driving force

The enthalpy change (ΔH) and entropy change (ΔS) are important thermodynamic parameters to understand the interactions of NCH and SA. The ΔH and ΔS can be calculated according to van't Hoff equation (Equation 5):

$$\ln K = -\frac{\Delta H}{RT} + \frac{\Delta S}{R} \qquad (5)$$

K is analogous to the effective quenching constants K_a at the same temperature and here we use the value of K_a. We could calculate ΔH from the slope of van't Hoff plot, while ΔS could be got from the intercept. All the detailed data of thermodynamic parameters are displayed in Table 2. Due to the similarity on structure, the results for HSA-NCH and BSA-NCH are analogical. As summarized by Ross and Subramanian of the thermodynamic law of judging the primary binding driving force,[21,29,32] $\Delta H > 0$ and $\Delta S > 0$ suggest that the primary driving force is hydrophobic interaction, while hydrogen bonds and van Der Waals force are not the dominating factors. It is reasonable because the molecules of NCH is made up of two hydrophobic phenyl moiety, while both HSA and BSA have some hydrophobic binding sites, such as the

well-known Sudlow I (so called Site I).

The change of Gibbs free energy (ΔG) is a crucial factor to the reaction tendency. The value of ΔG at different temperatures are calculated by Equation 6:

$$\Delta G = \Delta H - T\Delta S = -RT \ln K \quad (6)$$

As the quenching is actually a spontaneous process, the Gibbs free is negative ($\Delta G < 0$). Accordingly, the positive entropy change ($\Delta S > 0$) is favorable. However, the positive enthalpy change ($\Delta H > 0$) is unfavorable and harmful for the spontaneous interaction and rising the energy level of the NCH-SA complex. Therefore, based on the calculation of van't Hoff equation, NCH induced quenching of SA fluorescence is an entropy-driven spontaneous process. The large and favorable entropy change may be caused by micro-environmental change in the binding process, such as the secondary structure change of protein or de-solvent process in some region of protein.

3.3.3 Binding number and binding site

We employed the double-logarithmic equation (Equation 7) to calculate the possible binding number for NCH in SA.

$$\lg(\frac{F_0 - F}{F}) = \lg K_b + n \lg[Q] \quad (7)$$

According to Equation 7, a plot of log $[(F_0 - F)/F]$ vs. log $[Q]$ will give a straight line with slope equaling to *n,* the binding number. Take HSA-NCH as an example, Table 2 demonstrates a slightly changeable value of n , which is close to 1.2. This means that NCH binds strongly to HSA, independent upon a single binding site for NCH in HSA, while there may be another weak binding site. The binding number slightly increases

with the rising temperature, this may be a reasonable consequence that the peptide of HSA becomes more tender with the increasing temperature and exposes another binding site. The similar results comes up for BSA-NCH system.

So as to investigate and verify the precise binding site, site competitive replacement experiments were conducted at 298 K, and warfarin and ibuprofen were used as site marker owing to their specific binding in a known SA site. Warfarin specifically binds to Sudlow's site I and ibuprofen specifically binds to Sudlow's Site II.[1,9,11] In the site competitive replacement experiments, a continuous titration of NCH to a solution of SA-site marker(warfarin or ibuprofen) was conducted. The binding parameters will change if the competition of NCH and site markers really exist.

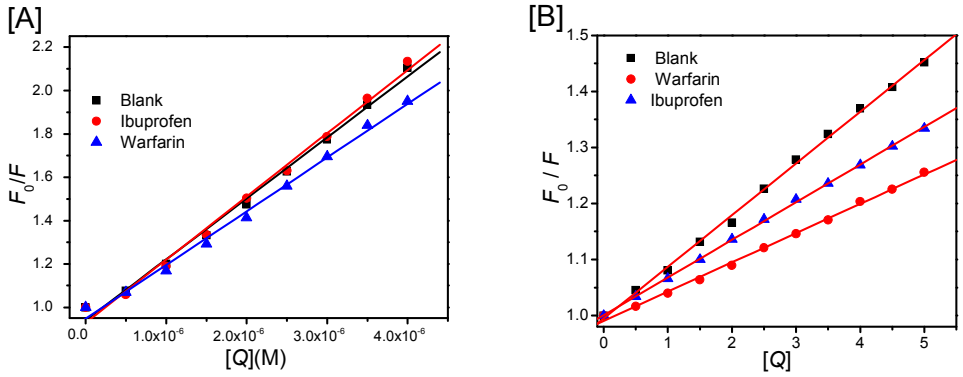

Fig. 6 The Stern-Volmer plots of HSA-NCH[A] and BSA-NCH[B] system in presence of site markers.

The quenching constants are calculated and compared to evaluate the influence of site marker, showed in Fig. 6. The quenching constant of just HSA-NCH system is about 1.19×10^5 L·mol^{-1} at 298 K, while that with warfarin and ibuprofen is 1.02×10^5 L·mol^{-1}, 1.20×10^5 L·mol^{-1}, respectively. The quenching constant with ibuprofen

is almost the same as without it, while that in the presence of warfarin is much smaller than its absence. These reveal the competition between NCH and warfarin or ibuprofen is not the same, and NCH mainly competes with warfarin in Sudlow's site I, whereas almost no competition is detected between NCH and ibuprofen, suggesting NCH mainly binds to HSA in Sudlow's site I.

The situation of BSA is a little different. The quenching constant of just BSA-NCH system is about 5.58×10^4 L·mol^{-1} at 298 K, while that with warfarin and ibuprofen is 3.82×10^4 L·mol^{-1}, 2.09×10^4 L·mol^{-1}, respectively. Both the quenching constants with warfarin and ibuprofen are smaller than that its absence. This indicates NCH compete with warfarin and ibuprofen together, but mainly competes with warfarin in Sudlow's site I. Herein, confirmed by the site competitive replacement experiments, we can ensure that NCH binds to SA in sub-domain IIA or called Sudlow's site I.

3.3.4 Conformational change

When drugs bind to SA, they usually cause conformational change of SA in secondary structure. This conformational change can be well-detected by circular dichroism spectroscopy(CD) and 3D fluorescence spectra.

The CD spectra of SA with various concentration of NCH at room temperatures are shown in Fig. 7. Both HSA and BSA exhibit two negative bands at 208 nm and 222 nm, which represent the typical α-helix structure of protein. With the presence of NCH, the shape and intensity of negative bands almost have no detectable change, expressing that the binding of NCH can't change the secondary structure especially

α-helix structure of protein in a significant way, only in a slight way. After the calculation[1], for HSA-NCH, we find that the content of α-helix changes slightly, from 0.569 to 0.550, while the content of unordered structure changes a little bit, from 0.371 to 0.392. For BSA-NCH, α-helix changes from 0.603 to 0.587, and unordered structure changes from 0.352 to 0.388. These results suggest NCH slightly destroys the native α-helix of SA and changes it into the unordered peptide.

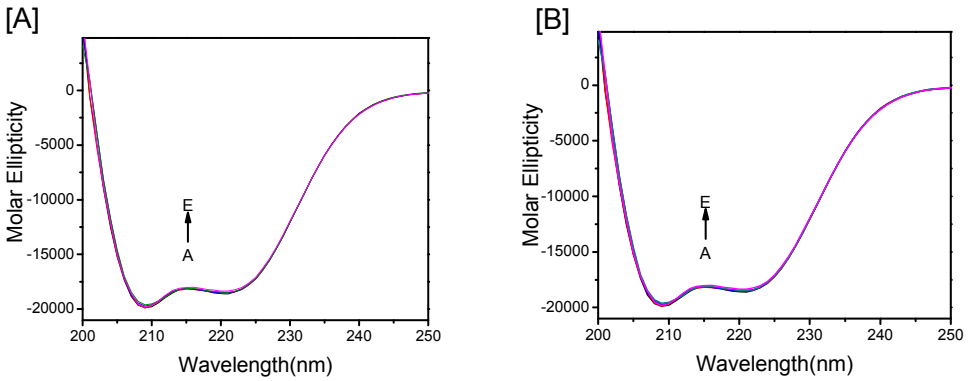

Fig. 7 Effect of NCH on the CD spectra of HSA[A] and BSA[B].

c(HSA) = c(BSA) = 10 μM; SA : NCH A→E: 1:0, 1:1, 1:2, 1:4, 1:8.

Table 3 The parameters of 3D fluorescence spectra of SA and NCH-SA

	HSA			HSA-NCH		
	Em(nm)	Ex(nm)	Ordinate	Em(nm)	Ex(nm)	Ordinate
Peak1	275	348.5	462.8	275	346	368.2
Peak2	220	345.5	397.4	220	340	291.2
	BSA			BSA-NCH		
	Em(nm)	Ex(nm)	Ordinate	Em(nm)	Ex(nm)	Ordinate
Peak1	280	349.0	487.1	280	348.0	311.6
Peak2	225	347.0	383.8	225	347.0	272.9

3D fluorescence spectroscopy is used to further study the conformational change of HSA more carefully. Fig. SI 6 shows the 3D fluorescence spectra for SA (Fig. SI 6[A]&[C]) and NCH-SA system (Fig. SI 6[B]&[D]).

There are four peaks in the 3D fluorescence spectra as showed in Fig. SI 6. The peak at left is Rayleigh scattering peak, whereas the one at right is second-ordered Rayleigh scattering peak. The intensity of the Rayleigh scattering is positive related to the particle size in the solution. Both the intensity of first-ordered and second-ordered Rayleigh scattering peak enhance slightly with the addition of NCH, suggesting that the diameter of the NCH-SA complex is a little larger than SA itself. Two strong fluorescence peaks are in the middle of the figure, marked with peak1 and peak2. Peak 1 mainly reveals the spectral behavior of tryptophan residue. Peak 2 dominatingly relates to the fluorescence spectral behavior of polypeptide backbone structure, and its intensity is correlated with the secondary structure of protein.[4,20] The corresponding parameters for Peak1 and Peak2 are listed in Table 3.

For HSA-NCH system, the fluorescence intensity of Peak 1 has been quenching about 20% with the addition of NCH, together with a slight blue shift of λ_{max}(about 2 nm), suggesting that NCH binds to HSA and the binding site is near the residue of tryptophan, and the binding changes the micro-environmental of tryptophan residue to a little more hydrophobic. The intensity of peak2 decreases significantly, about 26%, with the adding of NCH, while a notable blue shift (about 5 nm) is detected. This shows that the binding of NCH affects the peptide structure and this is in according to the calculation based on the CD spectra. The influence of NCH to BSA's 3D fluorescent spectra showed the similar results.

Based on the discussion above, the interaction of NCH with SA induces a slight change of the polypeptides of protein, destroying the native α-helix and turning into

unordered peptide.

3.4 Molecular docking study

Molecular docking is a common and widely used method dealing with interactions between biomacromolecules and organic ligands. Regarding NCH-SA interaction in this paper, by means of molecular docking, we can theoretically predict the binding site of NCH in SA, analyze the driving force of the binding at molecular structure level.

In order to evaluate the possible binding site of NCH in HSA, we docked NCH into each possible site of 2BXG and 1H9Z, using different parameters setting. The docking with the highest score was the most possible binding in this parameters setting. The highest score for each combination was showed in Fig. 8. The score here represents the binding strength of NCH towards HSA, and a high score stands for a strong binding and a stable complex.

As showed in Fig. 8[A]&[B], the dockings give low scores and different binding sites, indicating a weak and random binding in this situation. From Fig. 8[C]&[D], NCH almost bound to HSA in the same site and conformation under the AUTO and LIGAND mode in the same site of warfarin with a high score, which means a strong and independent binding. These four sets of docking together could theoretically prove that NCH possibly binds to HSA in the site of warfarin, or Sudlow's site I. And this is precisely identical with the results in site competitive replacement experiments.

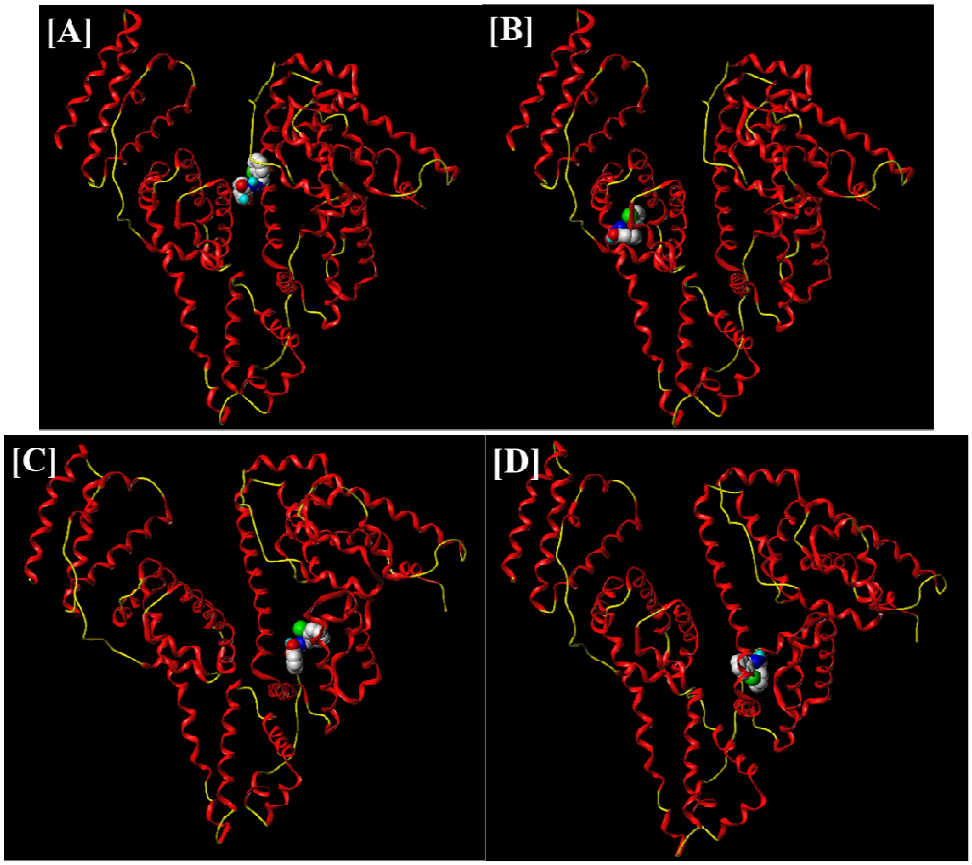

Fig. 8 The docking results of NCH and HSA system

[A]: The highest score in 2BXG with AUTO mode. Score:4.57. [B]: The highest score in 2BXG with LIGAND mode. Score:4,52. [C]: The highest score in 1H9Z with AUTO mode. Score:5.20. [D]: The highest score in 1H9Z with LIGAND mode. Score:5.87. NCH is shown in space-filling model, while HSA is showed in Tube and Ribbon mode.

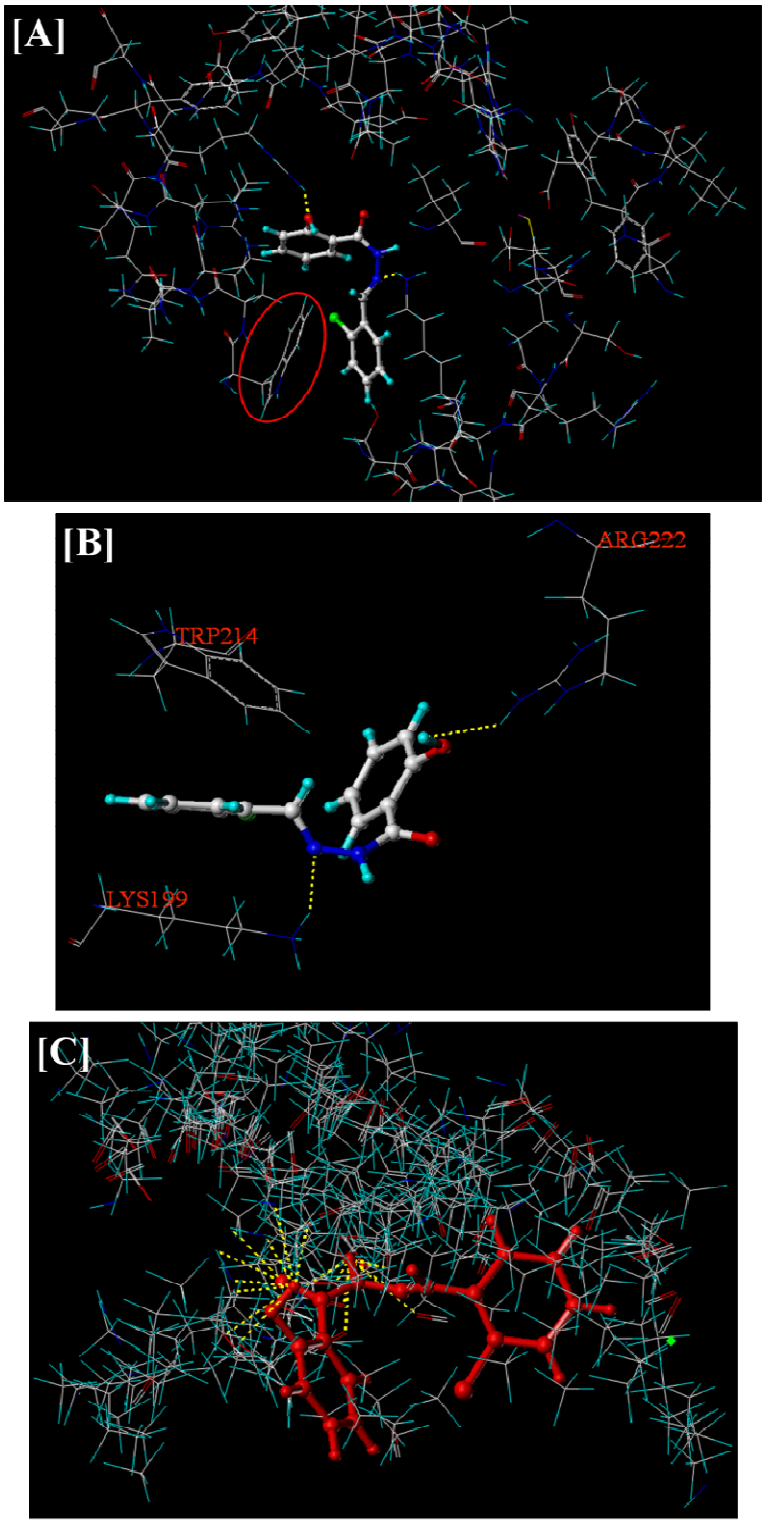

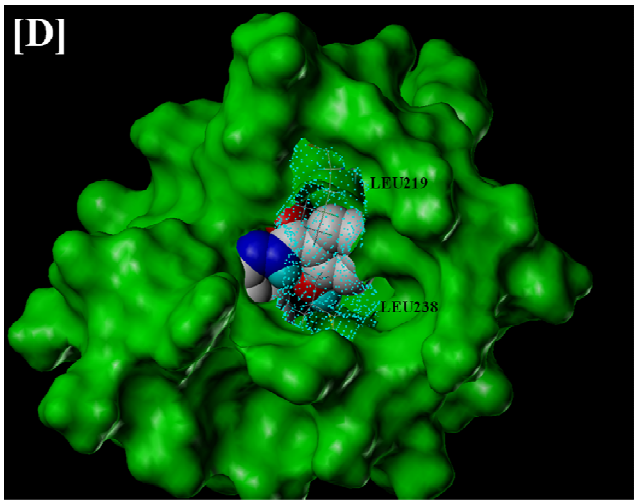

Fig. 9 The detailed docking results of NCH and HSA

[A]: The configuration of NCH in binding site of HSA. NCH is shown in ball-stick model, while Trp214 we concerned are showed in the red circle. All hydrogen bonds are showed as yellow dashed lines. [B]: The illustration of hydrogen bonds and the conformation of Trp214 and NCH. NCH is shown in ball-stick model. [C]:The align of NCH with the protomol. There are three kinds of probe: CH_4 for the hydrophobicity, C=O for hydrophilicity and hydrogen bond acceptor and N-H for hydrophilicity and hydrogen bond donor and acceptor. [D]:The illustration of the obstacle (blue dot Leu218 and Leu238 surface) in the entrance pathway of NCH into the binding site.

We apply the most possible binding model in Fig. 8[D] in analyzing the detailed binding pattern of NCH to HSA. The detailed docking results are shown in Fig. 9, including the position and configuration of NCH in the binding pocket, the interaction driving force and amino acid residues lying around.

The precise binding site of NCH in HSA is shown in Fig. 9[A]. NCH binds to HSA on Sudlow's site I, the same with Warfarin. The tryptophan 214 residue has been involved in the binding pocket and in a reasonable distance from NCH, so the binding

of NCH would seriously interfere the fluorescent and UV-visible spectra of HSA. Fig. 9[B] shows that the NCH forms two hydrogen bonds with the residues of HSA: O19 in NCH makes one H-Bond with HH21 in Arg222, and N9 in NCH forms one H-Bond with HZ2 in Lys199. The H-Bonds here help to fix the position of NCH and stabilize the NCH-HSA complex. The amino acid residues involved in binding pocket are comprised of Ser193, Leu198, Leu203, Ala210, Phe211, Ala215, Val216, Arg218, Leu219, Ser220, Leu238, Ile290, Ala291 and Glu292. As showed clear in Fig. 9[C], the 2-hydroxy-phenyl group in NCH inserts into a hydrophobic loop formed by Ala215, Val216, Leu219, Leu238 and Ala291, showed as the align of NCH with the crowded CH_4 probe in the right side of Fig. 9[C]. The 2-chlorophenyl group stretches to another hydrophobic loop made by Leu198, Leu203, Ala210 and Phe211. These two hydrophobic moieties are buried in pockets created by hydrophobic residue, making the molecule of NCH in a proper conformation to adapt the shape of the binding pocket. And as a result, the priority driving force of the interaction between NCH and HSA is the hydrophobic interaction, while the hydrogen bonds and van Der Waals force play a minor part. This is coincide with the discussion of driving force in above section. The residues Ile290, Ala291 and Glu292 are the very important residue that involved in the transition from the α-helix to the unordered ribbon, so the interaction of NCH to these important residues would affect the peptide especially the unordered ribbon.

The detailed docking results of NCH into BSA are showed clearly in Fig. SI 7. The fluorophore Trp237 residue has been involved in the binding site, so the binding of

NCH would seriously interfere the fluorescent and UV-visible spectra of BSA. Two hydrogen bonds have been observed in BSA-NCH system, H15 in NCH makes one hydrogen bond with His265.NE2, and another hydrogen bond with Tyr173.OH. The formation of hydrogen bonds stabilizes the complex of NCH and BSA and contributes to the 3D space position change of NCH to adapt the shape of the pocket of site I. 2-hydroxy-phenyl group in NCH inserts into a hydrophobic loop formed by Ile313, Ile287 and Leu242, while The 2-chlorophenyl group stretches to another hydrophobic loop made by Leu283, Leu261 and Ser310. The result here suggests the binding site of NCH on BSA is site I, and the mainly force in interaction is hydrophobic interaction.

Based on the analyze above, we could theoretically conclude that NCH binds to both HSA and BSA in Sudlow's site I and formed a stable complex. Hydrophobic interaction is the primary driving force. The binding of NCH would seriously interfere SA's fluorescent and UV-visible spectroscopy and secondary structure.

As to the unclassical static quenching in fluorescent study, the structural reason can be explained clearly by Fig. 9[D] and Fig. SI 7[D]. As showed in Fig. 9[D], the binding sites is deeply buried in the body of HSA. Before binding into the proper position in HSA, NCH have to pass through the channel formed by the amino acid residues outside the binding sites, Leu219 and Leu238, here. The only way for NCH to enter the pocket is pushing its way through Leu219 and Leu238 residue (showed in blue dots) lying in the middle of the pathway. This requires a large activation energy and increases the energy level of NCH-HSA complex. Moreover, the molecule of

NCH is rigid and can't change the shape to slide into the binding site. These together turn out to be the big activation energy of the binding process. As showed in Fig. SI 7[D], the same obstacle in BSA is composed of Arg218 and Glu315, and this requires a large E_a to overcome the blocking of these two residues to get into the binding site of BSA.

As concluded, the special structure of the binding pocket in SA and the rigid structure of NCH make the binding process a little difficult, therefore this binding process requires a larger E_a discussed in the above section, which at last caused the unclassical static quenching mechanism in the fluorescence study.

4. Conclusion

As discussed above, NCH, a novel acylhydrazone derivative, could be strongly adsorbed to SA in an equivalent and independent binding site in Sudlow's site I, inducing the quenching of SA's intrinsic fluorescence emission by an unclassical static quenching mechanism. The dominantly driving force of this interaction was hydrophobic interaction, whereas the hydrogen bonds help NCH to adapt the shape of the pocket in the binding site. While the binding induced the change of unordered ribbon of the secondary structure of protein. The big activation energy requirement for overcoming the blocking of amino acid residues in the binding process causes the unclassical quenching in fluorescent study. The results constituted a helpful guide in an attempt to unravel the mechanism of NCH-protein interactions, as well as the NCH analogy.

Acknowledgments

The authors gratefully acknowledge financial support of National Natural Science Foundation of China (Grant No.21173026, 20921062), Program for Changjiang Scholars and Innovative Research Team in University (IRT1030).

Electronic Supplementary Information Available: the control of EIS, the ^{1}H NMR, MS, IR spectra of NCH and addition UV-visible spectra, Langmuir isotherm plots, 3D fluorescence spectra for NCH-SA system, and detailed docking results of NCH and BSA.

References

1 F. Tian, F. Jiang, X. Han, C. Xiang, Y. Ge, J. Li, Y. Zhang, R. Li, X. Ding and Y. Liu, *J. Phys. Chem. B*, 2010, **114**, 14842–14853.

2 S. Rollas and Ş. Küçükgüzel, *Molecules*, 2007, **12**, 1910-1939.

3 D. Lovejoy and D. Richardson , *Blood*, 2002, **100**, 666-676.

4 D. Kalinowski, P. Sharpe, P. Bernhardt and D. Richardson, *J. Med. Chem.*, 2007, **50**, 6212-6225.

5 S. Kucukguzel, E. Oruc, S. Rollas, F. Sahin and A. Ozbek, *Eur. J. Med. Chem.*, 2002, **37** 197-206.

6 D. Himmel, S. Sarafianos, S. Dharmasena, M. Hossain, K. McCoy-Simandle, T. Ilina, A. Clark, J. Knight, J. Julias, P. Clark, K. Krogh-Jespersen, R. Levy, S. Hughes, M. Parniak and E. Arnold, *ACS Chem. Biol.*, 2006, **1**, 702-712.

7 J. Dimmock, S. Vashishtha and J. Stables, *Eur. J. Med. Chem.*, 2000, **35**, 241-248.

8 L. Bukowski, M. Janowiec, Z. Zwolska-Kwiek and Z. Andrzejczyk, *Pharmazie*, 1999, **54**, 651-654.

9 D. Kalinowski, P. Sharpe, P. Bernhardt and D. Richardson, *J. Med. Chem.*, 2008, **51**, 331–344.

10 D. Kalinowski and D. Richardson, *Pharmacol. Rev.*, 2005, **57**, 547–583.

11 Y. Yu, D. Kalinowski, Z. Kovacevic, A. Siafakas, P. Jansson, C. Stefani, D. Lovejoy, P. Sharpe, P. Bernhardt, D. Richardson, *J. Med. Chem.*, 2009, **52**, 5271–5294.

12 Y. Hu, Y. Liu, T. Sun, A. Bai, J. Lu and Z. Pi, *Int. J. Biol. Macromol.*, 2009, **39**, 280–285.

13 C. Yang, P. Mei, Z. Guan and Y. Liu, *Chin. J. Chem.*, 2007, **25**, 1085–1089.

14 C. Yang, Y. Liu, D. Zheng, J. Zhu and J. Dai, *J. Photochem. Photobiol. A*, 2007, **188**, 51–55.

15 J. Tian, J. Liu, W. He, Z. Hu, X. Yao and X. Chen, *Biomacromolecules*, 2004, **5**, 1956-1961.

16 D. Shcharbin, E. Pedziwiatr, L. Chonco, J. Bermejo-Martı´n, P. Ortega, F. Mata, R. Eritja, R. Go´mez, B. Klajnert, M. Bryszewska and M. Mun˜oz-Fernandezand, *Biomacromolecules*, 2007, **8**, 2059-2062.

17 B. Zhou, Z. Zhang, Y. Zhang, R. Li, Q. Xiao, Y. Liu and Z. Li, *J. Pharm. Sci.*, 2009, **98**, 105-113.

18 R. Beauchemin, C. N'soukpoé-Kossi, T. Thomas, T. Carpentier and H. Tajmir-Riahi, *Biomacromolecules*, 2007, **8**, 3177–3183.

19 Y. Hu, Y. Ou-Yang, C. Dai, Y. Liu and X. Xiao, *Biomacromolecules*, 2010, **11**, 106–112.

20 Y. Zhang, J. Dai, X. Zhang, X. Yang and Y. Liu, *J. Mol. Struct.*, 2008, **888**, 152–159.

21 Y. Zhang, X. Xiang, P. Mei, J. Dai, L. Zhang and Y. Liu, *Spectrochim. Acta, Part A*, 2009, **72**, 907–914.

22 R. Li, F. Jiang, Q. Xiao, J. Li, Q. Yu, Y. Liu and C. Zeng, *Nanotechnology*, 2010, **21**, 475102.

23 F. Tian, J. Li, F. Jiang, X. Han, C. Xiang, Y. Ge, L. Li and Y. Liu, *RSC Adv.*, 2012, **2**, 501 - 513

24 J. Lakowicz, *Principles of Fluorescence Spectroscopy, 2nd ed., Plenum*, New York, 1999.

25 V. Bernard, *Molecular Fluorescence: Principles and Applications*, Wiley-VCH, Weinheim, 2001.

26 Q. Xiao, S. Huang, Y. Liu, F. Tian and J. Zhu, *J. Fluoresc.*, 2009, **19**, 317-326.

27 J. Demas and J. Addington, *J. Am. Chem. Soc.*, 1974, **96**, 3663–3664.

28 A. Vaiana, H. Neuweiler, A. Schulz, J. Wolfrum, M. Sauer and J. Smith, *J. Am. Chem. Soc.*, 2003, **125**, 14564-14572.

29 Y. Hu, Y. Liu, J. Wang, X. Xiao and S. Qu, *J. Pharm. Biomed. Anal.*, 2004, **36**, 915–919.

30 B. Sahoo, K. Ghosh and S. Dasgupta, *Biopolymers*, 2008, **91**, 108–119.

31 J. Chen, X. Jiang, X. Chen and Y. Chen, *J. Mol. Struct.*, 2008, **876**, 121–126.

32 X. Han, P. Mei, Y. Liu, Q. Xiao, F. Jiang and R. Li, *Spectrochim. Acta, Part A*, 2009, **74**, 781–787.

33 A. Barik, B. Mishra, A. Kunwar and K. Priyadarsini, *Chem. Phys. Lett.*, 2007, **436**, 239–243.

34 D. Li, X. Zou, Q. Shen and S. Dong, *Electrochem. Commun.*, 2007, **9**, 191–196.

35 Y. Ge, S. Tai, Z. Xu, L. Lai, F. Tian, D. Li, F. Jiang, Y. Liu and Z. Gao, *Langmuir*, 2012, **28**, 5913–5920.